Materials Science and Engineering A 527 (2010) 4161–4168

Contents lists available at ScienceDirect

Materials Science and Engineering A

journal homepage: www.elsevier.com/locate/msea

Microstructure and texture evolution in dual-phase steels: Competition between recovery, recrystallization, and phase transformation

N. Peranio*, Y.J. Li, F. Roters, D. Raabe

Max-Planck-Institute for Iron Research GmbH, Max-Planck-Strasse 1, 40237 Düsseldorf, Germany

ARTICLE INFO

Article history:
Received 9 November 2009
Received in revised form 6 March 2010
Accepted 9 March 2010

Keywords:
Steel
EBSD
Microanalysis
Thermomechanical processing
Recrystallization
Phase transformation

ABSTRACT

The microstructure and texture evolution of dual-phase steel sheets with a cold reduction of about 50%, annealed at ferritic and intercritical temperatures, were analyzed by scanning electron microscopy and electron backscatter diffraction. The competition between recrystallization and phase transformation was of particular interest. The sheets were annealed in salt bath or were annealed in a MULTIPAS annealing simulator under variation of annealing temperature, annealing time, and heating rate. For low intercritical temperatures, recrystallization occurred before phase transformation. The sheets showed a similar through-thickness texture inhomogeneity with a plane-strain texture with strong α-fiber and weak γ-fiber as cold rolled sheets and a ferritic–martensitic band structure in the sheet center layers. An inverse correlation between the volume fractions of recrystallized ferrite and martensite was observed. This interdependence is attributed to a different phase transformation kinetics for recyrstallized and deformed ferrite and is discussed in terms of deformation strain energy, diffusion, and number of nucleation sites.

1. Introduction

Carbon–manganese dual-phase steels are known for their combination of high strength and good formability, and therefore, are prospective materials for the automotive industry to achieve low energy consumption through weight reduction [1,2]. The results presented here are part of a series of analyses of microstructure evolution in hot rolled, cold rolled, and annealed sheets of dual-phase steels. One important step of thermal treatment of dual-phase steels is an intercritical annealing which converts the initial ferritic–pearlitic microstructure of cold rolled materials in a ferritic–martensitic microstructure after annealing. In the literature, microstructure analyses on dual-phase steels were published which covered the average texture evolution [3–7] and the morphology [8–10] of the constituents. The volume fractions of the constituents, their texture and morphologies are known to be determined by recovery, recrystallization, and phase transformation during intercritical annealing [1,11,12]. The competition between these mechanisms is determined by basic annealing parameters such as heating rate, intercritical annealing temperature, annealing time, cooling rate, and the final annealing temperature [2,8,12,13]. However, there is still little understanding about the competition between recrystallization and phase transformation and their driving forces [1,8,11,14].

Preliminary microstructure analyses of hot and cold rolled sheets of dual-phase steels yielded (i) a through-thickness texture inhomogeneity typical for BCC-steels [15] and (ii) a continuous through-thickness change of ferrite–pearlite spatial distribution from ferrite–pearlite band structure in the center to a heterogeneous distribution at the surface of the sheets. Therefore, in general the mechanical properties of the sheets before and after annealing are expected to be anisotropic and to depend on the through-thickness position. Annealing at high intercritical and particularly at austenitic temperatures yielded in the entire sheet a homogeneous texture, a heterogeneous distribution of the constituents, and thereby no dependence of the mechanical properties on the through-thickness position. For high annealing temperatures, the driving force for microstructure evolution was mainly attributed to a reduction in free enthalpy during phase transformation. The microstructure analyses of hot and cold rolled sheets and of sheets annealed at high intercritical and at austenitic temperatures will be presented elsewhere.

In this work, annealing was applied at ferritic and low intercritical temperatures. At these low annealing temperatures, recrystallization and phase transformation should depend on details of the microstructure in the different through-thickness positions, and therefore, inhomogeneities with respect to microstructure and mechanical properties are less likely to be eliminated by annealing. The aim of this work is to study the dependence of microstructure evolution on strain introduced by deformation, on texture, and on morphology and distribution of the constituents in dual-phase steels annealed at low intercritical temperatures.

* Corresponding author. Tel.: +49 211 6792 393; fax: +49 211 6792 333.
E-mail address: n.peranio@mpie.de (N. Peranio).

0921-5093/$ – see front matter © 2010 Elsevier B.V. All rights reserved.
doi:10.1016/j.msea.2010.03.028

Table 1
Sample overview.

No.	Sample preparation	Sheet thickness (mm)	Annealing temperature (°C)	Annealing time (s)	Heating rate (K/s)	Cooling rate (K/s)
1	Salt bath	1.75	620, 635, 650, 665, 680, 695	10–5000		
2	Salt bath	1.75	710, 725, 740, 770, 800, 830	10–1500		
3	Salt bath	1.75	740	100, 200, 300		
4	Annealing simulator	1.75	740	100, 200, 300	20	−15
5	Annealing simulator	1.75	740	30	7, 20, 50	−15

2. Experimental

2.1. Sample overview

A sample overview is given in Table 1. The starting material was hot rolled sheets with a thickness of 3.75 mm. Preliminary metallurgical measurements yielded volume fractions of about 65% ferrite and 35% pearlite. The sheets had a chemical composition of 0.147 wt.% C, 1.868 wt.% Mn, 0.403 wt.% Si, and smaller amounts of other alloying elements. The sheets were then industrially cold rolled to a thickness of 1.75 mm. Details about the chemical composition and the microstructure of the hot and cold rolled sheets are given elsewhere.

In general, the annealing procedure for dual-phase steels can roughly be subdivided in (i) intercritical annealing followed by (ii) annealing at temperatures slightly below the martensite start temperature [2]. In this work, the cold rolled sheets were systematically annealed omitting the second annealing step (samples 1–5). For this, annealing in salt bath or in a MULTIPAS® annealing simulator was applied under variation of the annealing temperature, the annealing time, and the heating rate. The annealing simulator is based on direct resistance heating.

First, sheets were annealed in salt bath and quenched in water at a fine temperature–time schedule and a wide annealing time range (samples 1 and 2). For these samples, only the hardness in dependence of annealing time was measured. At ferritic temperatures of $T < A_{c1}$ (samples 1), the competition between recovery and recrystallization was of interest. At intercritical temperatures of $A_{c1} < T < A_{c3}$ (samples 2), the competition between recrystallization and phase transformation should be analyzed in more detail.

Second, the sheets were annealed in the annealing simulator or annealed in salt bath at an intercritical annealing temperature of 740 °C (samples 3 and 4). The annealing times were 100 s, 200 s, and 300 s. The aim was to get an overview of the effects of annealing temperature and annealing time on microstructure evolution at low intercritical annealing temperature slightly above A_{c1}.

Finally, the sheets were annealed in the annealing simulator at 740 °C for 30 s under variation of the heating rate (samples 5), the cooling rates being identical with samples 4. The aim was to study the effect of the heating rate on the competition between recovery and recrystallization.

2.2. Hardness measurements, conventional SEM, and EBSD

The hardness was determined according to Vickers (HV5) at the surface of the sheets and in the center of transverse sections of the sheets. The indentations had a diameter of at least 140 μm, and therefore, at least 500 ferrite grains were deformed for one single hardness measurement.

Structural, chemical, and texture analyses were carried out by scanning electron microscopy (SEM) combined with energy dispersive X-ray spectrometry (EDX) and electron backscatter diffraction (EBSD). A field emission SEM (Jeol JSM 6500 F) was used operated at an accelerating voltage of 15 kV. The microscope is equipped with a DigiView EBSD detector combined with the OIMDC EBSD analysis program provided by TSL/EDAX. Transverse and longitudinal sections of the sheets were prepared followed by conventional metallographic sample preparation including grinding, polishing, and etching. After conventional SEM analyses, the samples were mechanically polished once again and final polished with a suspension of 0.1-μm diameter silica particles for EBSD measurements. The EBSD measurements showed no significant polishing artifacts [16]. Finally, a single iteration grain dilation clean-up was applied on the measurement data using a grain tolerance angle of 3° and a minimum grain size of five measurement points. The clean-up procedure usually affected less than 5% of the measurement points.

The samples were etched for 10 s with 1% Nital for analysis of the grain structure and for the determination of the distribution and the volume fractions of the constituents. The microstructures were first conventionally analyzed in the SEM by imaging with secondary and backscattered electrons. The secondary electron signal is useful to distinguish pro-eutectoid ferrite, pearlite, and martensite. These constituents differ in etching rates, and therefore, yielded a strong topography contrast. The backscattered electron signal is useful to distinguish recovered and recrystallized pro-eutectoid ferrite, since they differ with respect to in-grain orientation gradients introduced by dislocations, and therefore, yielded a strong orientation contrast. A grid method was used for the determination of the volume fractions of the constituents (4000 grid sites, 2 μm grid spacing).

The constituents in dual-phase steels can be distinguished by EBSD on the basis of following parameters, which are being explained in more detail elsewhere. (i) The Image Quality (IQ) parameter depends on distortions of the crystal lattice. (ii) The Kernel Average Misorientation (KAM) and (iii) the Grain Orientation Spread (GS) are large in regions with large orientation gradients which indicate a large density of geometrically necessary dislocations [16,17]. Cold rolled ferrite, recovered ferrite, pearlite, and martensite yielded small IQ, large KAM, and large GS values. Recrystallized ferrite and ferrite after phase transformation showed large IQ, small KAM, and small GS values.

A KAM value smaller than 0.5° was used to quantitatively determine the volume fractions of recrystallized ferrite and ferrite after phase transformation [16]. Particularly, a GS value smaller than 1.5° was used to separate and quantitatively analyze the morphology of recrystallized ferrite grains or ferrite grains after phase transformation. A grid method was applied on IQ maps for the determination of the volume fraction of martensite. The sheets also showed retained austenite after intercritical annealing. The volume fraction of retained austenite was less than 1%, and therefore, was not further considered.

Two types of EBSD measurements were applied. (i) The average texture, where all constituents were included, was measured in transverse sections of the sheets in a region extending from the center ($s = 0$) to the surface ($s = 1$) of the sheets [18]. The through-thickness parameter s specifies the position in the sheet where $s = a/(d/2)$ with a being the spacing between the layer inspected and the center layer and d the sheet thickness [15,19]. The measurement area had a width of 700 μm in transverse direction (TD) and a height of at least 1000 μm in normal direction (ND). Only measurements points with a Confidence Index (CI) larger than 0.05 were considered. For a determination of the texture in dependence of the through-thickness position s, the total area was subdivided in 700 μm × 100 μm large slices in normal direction. Within each slice about 3000 grains contributed to the texture analysis, since

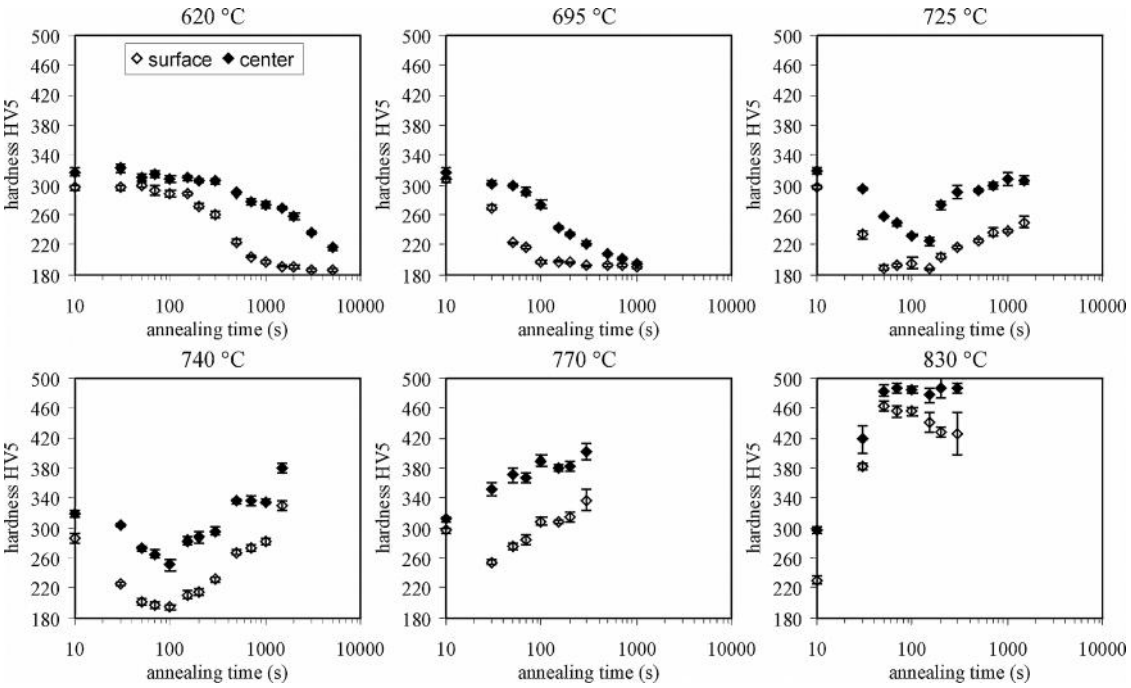

Fig. 1. Hardness in dependence of the annealing time measured in the center and at the surface of the sheets. The sheets were annealed in salt bath at ferritic and intercritical annealing temperatures.

the average ferrite grain size was 5 μm and the step size for EBSD measurements was 1.5 μm. (ii) EBSD was carried out in the center and at the surface of transverse and longitudinal sections of the sheets at high lateral resolution with a step size of 0.2 μm. Therefore, the texture and morphology of all constituents could separately be analyzed. The measurement areas had a size of 80 μm in normal direction and 200 μm in transverse or rolling direction, respectively. In general, grains were defined by a minimum of five measurement points with a CI value larger than 0.05 surrounded by grain boundaries with angles of at least 3°. In this work, the average grain sizes determined by EBSD are area-weighted values, i.e., the average grain size is the sum of grain sizes each multiplied with the corresponding grain areas and divided by the sum of grain areas.

3. Results

3.1. Hardness after annealing in the ferritic temperature range

The cold rolled sheets were annealed in salt bath using a fine temperature–time schedule with ferritic annealing temperatures between 620 °C and 695 °C (Table 1, samples 1). Only the hardness was measured on these samples. The hardness in dependence of annealing time is shown in Fig. 1 only for extreme annealing temperatures of 620 °C and 695 °C. As expected, (i) the hardness first decreased slightly due to recovery and then significantly due to recrystallization and (ii) the incubation and recrystallization times decreased for increasing annealing temperatures. However, the incubation and recrystallization times were smaller at the surface than in the center of the sheets. In summary, recrystallization was faster at the surface than in the center of the sheets.

3.2. Hardness after annealing in the intercritical temperature range

The sheets were intercritically annealed in salt bath, a fine temperature–time schedule with annealing temperatures between 710 °C and 830 °C was applied (Table 1, samples 2). The hardness in dependence of annealing time was first determined at the surface of the sheets (Fig. 1).

At an annealing temperature of 725 °C, the hardness immediately decreased to a value of about 190 HV5 within the first 50 s and remained constant up to an annealing time of 150 s. The decrease of hardness with annealing time at the beginning of intercritical annealing is very similar to an annealing at a ferritic temperature of 695 °C. Particularly, the hardness minimum is identical with the hardness after recrystallization at ferritic temperatures. Therefore, for an annealing temperature of 725 °C the results indicate a full recrystallization at the surface within the first 50 s. For annealing times larger than 150 s the hardness continuously increased with annealing time. This indicates an on going phase transformation and thereby an increase of the volume fraction of martensite after quenching. At an annealing temperature of 740 °C the hardness in dependence of annealing time is similar to the annealing at 725 °C. However, phase transformation started immediately after recrystallization was completed.

For an annealing temperature of 770 °C the hardness at the surface showed after 30 s a minimum of about 255 HV5, being larger than the hardness minimum found at 740 °C. Therefore, recrystallization was not completed when phase transformation started. Finally, at an annealing temperature of 830 °C the hardness already decreased to 230 HV5 after an annealing time of 10 s. Thereafter, the hardness increased to about 460 HV5 after 50 s, which is significantly larger than the hardness found in cold rolled sheets, and therefore, indicates an almost pure martensitic microstructure. In summary, at the surface of the sheets the incubation time for phase transformation decreased with increasing annealing temperature and yielded a strong overlap of recrystallization and phase transformation for intercritical annealing temperatures larger than 740 °C.

The hardness in dependence of annealing time was also measured in the center of the sheets and showed common features with results obtained at the surface of the sheets (Fig. 1). However, at annealing temperatures of 725 °C and 740 °C the hardness decreased slower in the center than at the surface of the sheets. Also, the hardness minimum was found to be about 250 HV5, which

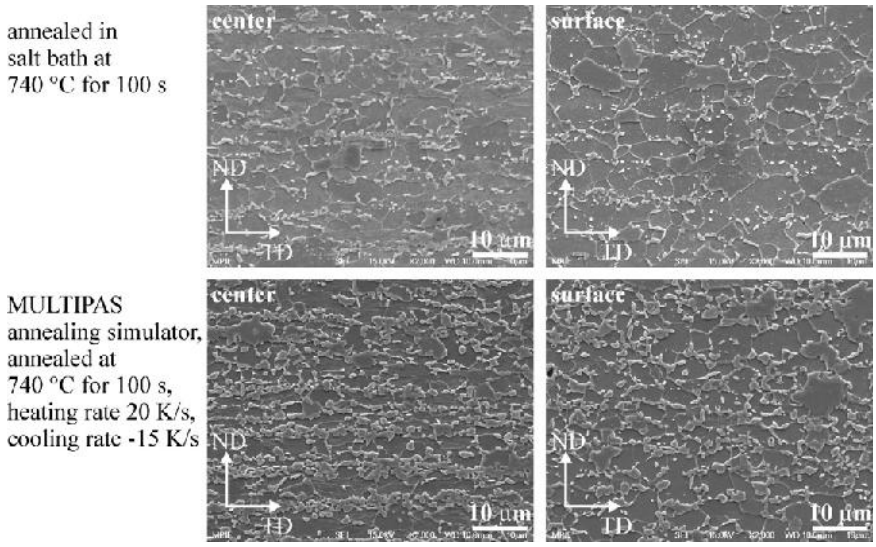

Fig. 2. Scanning electron microscopy on transverse sections of sheets intercritically annealed in salt bath and in the annealing simulator. The images were acquired in the center and at the surface of the sheets.

is significantly larger than the hardness minimum found at the surface of the sheet, and therefore, indicates partial recrystallization.

3.3. Microstructure after intercritical annealing in salt bath

Sheets were annealed in salt bath at an intercritical temperature of 740 °C for annealing times of 100–300 s (Table 1, samples 3). SEM analysis yielded a ferritic–martensitic microstructure (Fig. 2). Data about morphology and volume fractions of the constituents are given in Table 2. In the center of the sheets, ferrite and martensite were found to be distributed in bands along the rolling direction whereas at the surface both constituents were heterogeneously distributed. Martensite showed a granular morphology with a size of 1.5 μm, for all annealing times and in the entire sheet. The volume fraction of martensite was found to be larger in the center than at the surface of the sheets (Table 2). Ferrite was found to be almost fully recrystallized at the surface and only partially recrystallized in the center of the sheets. Recrystallized ferrite grains showed an almost equiaxed shape at size of 5 μm, independent of annealing time and through-thickness position in the sheet. The volume fraction of recrystallized ferrite did not significantly change for annealing times 100–300 s whereas the volume fraction of martensite clearly increased, which is in agreement with an increase of the hardness (Fig. 1). The correlation between hardness, volume fraction of martensite, and annealing time is shown in Fig. 3. The annealed sheets revealed after an annealing time of 100 s a volume fraction of 5% pearlite, which means that the pearlite–austenite phase transformation was still incomplete. The pearlite was mostly spherodized. Finally, precipitates were observed which were already present in hot and cold rolled sheets.

The results of EBSD analysis can be summarized as follows:

(i) A through-thickness texture inhomogeneity (Fig. 4) was found, being similar with the texture observed in cold rolled sheet. In the center of the sheet, a plane-strain texture with a strong α-fiber and a weak γ-fiber was observed (Fig. 4). Particularly, the texture component $\{1\,1\,2\}\ \langle 1\,\bar{1}\,0\rangle$ of the α-fiber showed a strong maximum in the center of the sheet. The texture at the surface and in the center of the sheet showed similar features. The main difference are less pronounced texture components $\{0\,0\,1\}\ \langle 1\,\bar{1}\,0\rangle$ and $\{1\,1\,2\}\ \langle 1\,\bar{1}\,0\rangle$ of the α-fiber at the surface of the sheet. In summary, in the center of the sheets the orientation fibers showed only a slight change after annealing. The reason is, that the texture in the center of the sheet was governed by recovered ferrite whereas the volume fraction of recrystallized ferrite is quite small (Table 2).

(ii) The in-grain orientation gradients differed significantly for recovered and recrystallized ferrite (Fig. 5). Compared to recrystallized ferrite, recovered ferrite and martensite yielded small IQ and large KAM values, and therefore, could be qualitatively easily distinguished from recrystallized ferrite. Recrystallized ferrite showed a small KAM value since the dislocation density and thereby the in-grain orientation gradients had dropped. The equiaxed shape of recrystallized ferrite grains can be clearly seen in the Inverse Pole Figure (IPF) maps (Fig. 5).

3.4. Microstructure after intercritical annealing in the annealing simulator

Annealing in the annealing simulator was carried out at an intercritical temperature of 740 °C for annealing times of 100–300 s (Table 1, samples 4). Sheets annealed in the annealing simulator and corresponding sheets annealed in salt bath (Table 1, samples 3) showed similar microstructures. (i) Ferrite was almost fully

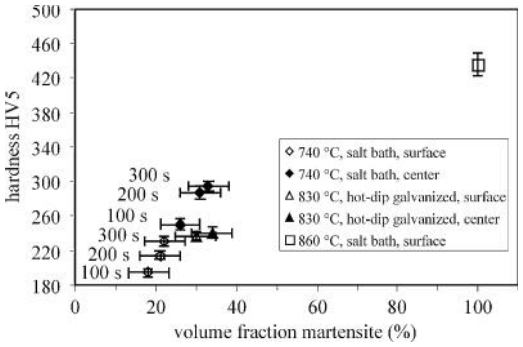

Fig. 3. Hardness in dependence of the martensite volume fraction of annealed sheets. The hardness was measured in the center and at the surface of sheets (i) annealed in salt bath at 740 °C for 100–300 s, (ii) industrially hot-dip galvanized at 830 °C for 80 s, and (iii) annealed in salt bath at 860 °C for 100 s.

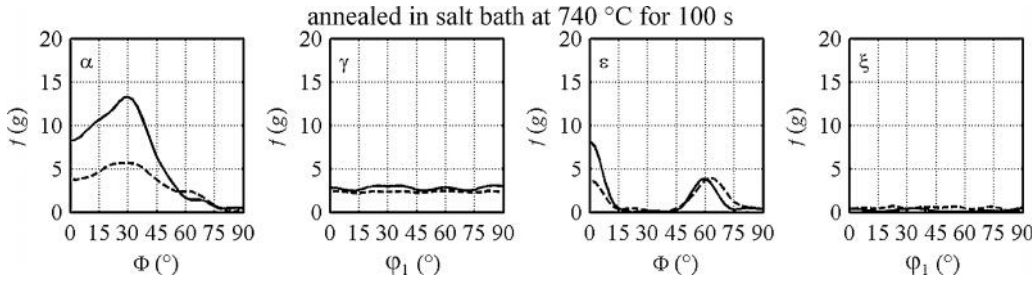

Fig. 4. Orientation density $f(g)$ along the α-, γ-, ε-, and ξ-fibers in dependence of the through-thickness position s in a sheet annealed in salt bath at intercritical temperature. The solid fiber line was obtained in the center ($s = 0$) and the dashed line was obtained at the surface ($s = 1$) of the sheet.

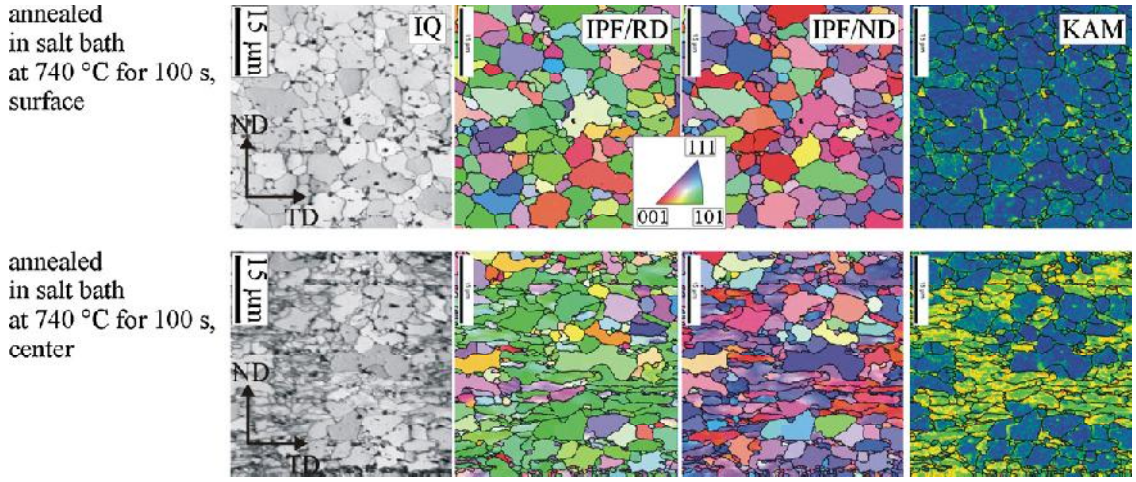

Fig. 5. EBSD carried out in the center and at the surface of a transverse section of a sheet annealed in salt bath. The images show the Image Quality map (IQ), the Inverse Pole Figure maps (IPF/RD and IPF/ND), and the Kernel Average Misorientation map (KAM, blue: $KAM = 0°$, red: $KAM = 3°$) obtained at the same specimen area. Grain boundaries with angles larger than 3° are indicated by black lines in the IPF and KAM maps.

recrystallized at the surface and only partially recrystallized in the center of the sheets (Fig. 2). (ii) The volume fraction of recrystallized ferrite did not increase for annealing times 100–300 s whereas the volume fraction of martensite increased (Table 2). (iii) The through-thickness texture inhomogeneity was almost the same for both samples. However, sheets annealed in salt bath revealed in the center and at the surface a significantly larger volume fraction of recrystallized ferrite and a smaller volume fraction of martensite compared to sheets annealed in the annealing simulator (Table 2).

3.5. Effect of heating rate on recrystallization

The dependence of the volume fraction of recrystallized ferrite on the heating rate was studied on sheets annealed in the annealing simulator at 740 °C for 30 s and heating rates between 7 K/s and 50 K/s (Table 1, samples 5). Sheets annealed in salt bath showed for this annealing time a large recrystallization rate (Fig. 1), and therefore, an annealing time of 30 s should be very sensitive to heating rate. In the through-thickness center layer, the volume fraction of recrystallized ferrite was found to be about 11% for a heating rate of

Table 2
Morphology measured in the center and at the surface of intercritically annealed sheets. The grain size of recrystallized (recr.) ferrite is given in (height || ND) × (width || TD) × (length || RD). Values written without brackets were determined by conventional SEM and values written in brackets were determined by EBSD.

Annealing parameters	Volume fractions recr. ferrite/martensite (%)		Grain size recr. ferrite (μm)	
	Center	Surface	Center	Surface
Samples 3, salt bath at 740 °C				
Annealing time 100 s	29/26 (32/21)	74/18 (85/15)	4.1 × 6.6 × 7.6 (1.8 × 3.9 × 4.9)	4.7 × 6.6 × 6.7 (2.0 × 4.2 × 4.5)
Annealing time 200 s	31/31	74/21	4.6 × 7.0 × NN	4.5 × 6.1 × NN
Annealing time 300 s	32/33	70/22	4.7 × 7.2 × NN	4.8 × 6.6 × NN
Samples 4, annealing simulator at 740 °C, heating rate 20 K/s, cooling rate −15 K/s				
Annealing time 100 s	11/45 (23/36)	49/39 (67/29)	3.0 × 4.3 × NN (1.3 × 2.7 × NN)	3.3 × 4.5 × NN (1.6 × 3.3 × NN)
Annealing time 200 s	14/48	48/42	3.2 × 4.5 × NN	3.5 × 4.6 × NN
Annealing time 300 s	10/53	38/52	3.0 × 4.2 × NN	3.3 × 4.4 × NN
Samples 5, annealing simulator at 740 °C for 30 s, cooling rate −15 K/s				
Heating rate 7 K/s	11/40	56/24	4.0 × 5.8 × NN	3.9 × 5.3 × NN
Heating rate 22 K/s	9/28	60/22	3.6 × 5.2 × NN	4.2 × 5.6 × NN
Heating rate 50 K/s	6/30	38/36	3.9 × 5.5 × NN	3.7 × 5.2 × NN
Samples 2, salt bath at 740 °C for 30 s				
Annealing time 30 s	3/0 (12/0)	56/0 (69/0)	2.8 × 3.9 × 4.7 (1.2 × 2.7 × NN)	3.7 × 4.9 × 5.2 (1.6 × 3.4 × NN)

7 K/s and 6% for a heating rate of 50 K/s (Table 2). Sheets annealed in salt bath at 740 °C for 30 s (samples 2) revealed a volume fraction of recrystallized ferrite of 3% (Table 2). Hence, the volume fraction of recrystallized ferrite decreased with the heating rate. At the surface of the sheets recrystallization was almost completed after 30 s of annealing for all heating rates, and therefore, the volume fraction of recrystallized ferrite did not depend on the heating rate (Table 2).

However, the heating rate also strongly affected the phase transformation of pearlite. Sheets annealed in salt bath at 740 °C for 30 s (samples 1) yielded a pure ferritic–pearlitic microstructure whereas annealing in the annealing simulator at the same temperature and for the same annealing time yielded an almost pure ferritic–martensitic microstructure at a martensite volume fraction of about 30% in the entire sheet.

4. Discussion

4.1. Preservation of through-thickness texture inhomogeneity and band structure after annealing at low intercritical temperatures

The annealing experiments yielded recovery, recrystallization, and phase transformation. Recovery was attributed to a slight reduction of hardness at the beginning of annealing at ferritic temperatures (Fig. 1). Recrystallization was proven by (i) a strong reduction of hardness obtained by annealing at ferritic temperatures and at the beginning of intercritical annealing for low temperatures up to 740 °C (Fig. 1) and (ii) by the observation of new equiaxed ferrite grains with small orientation gradients (Fig. 5). Phase transformation at intercritical temperatures was indicated by (i) an increase of hardness after a sufficiently long annealing time (Figs. 1 and 3) and (ii) the formation of martensite (Fig. 2).

Recrystallization was most pronounced at ferritic and low intercritical temperatures up to 740 °C, whereas at higher annealing temperatures phase transformation dominated over recrystallization (Fig. 1). Recrystallization yielded no change of the distribution of the constituents, i.e., the band structure in the center and the heterogeneous distribution of the constituents at the surface of the sheets were preserved (Fig. 2). The through-thickness texture inhomogeneity was also not effected at low intercritical annealing temperatures (Fig. 4). In other words, rolling texture and recrystallization texture were found to be similar which is well known from other materials such as aluminum [12]. However, recrystallization yielded a strong effect on the through-thickness dependence of the hardness since full recrystallization was obtained at the surface and only partial recrystallization in the center of the sheets (Figs. 1 and 5). The ratio of the hardness in the center to the hardness at the surface of the sheet increased from 1.06 after cold rolling to 1.29 after intercritical annealing at 740 °C for 100 s (Fig. 3).

4.2. Competition between recovery and recrystallization

In the last sections of this paper the competition between recovery, recrystallization, and phase transformation will be discussed in terms of driving forces and the manipulation of the balance of the constituents via the annealing parameters, i.e., annealing temperature, annealing time, heating rate, and cooling rate.

Recovery and recrystallization were found to be dominant for annealing at ferritic temperatures and at low intercritical temperatures up to 740 °C. The results showed several characteristic features which can be explained as follows:

(i) Recrystallization time decreased with increasing annealing temperature (Fig. 1), which confirms a thermally activated process and is usually explained by the Johnson–Mehl–Avrami–Kolmogorov (JMAK) model for recrystallization.

(ii) Incubation and recrystallization times were smaller at the surface than in the center of the sheets (Fig. 1). Particularly, full recrystallization occurred at the surface and partial recrystallization in the center of the sheets (Fig. 5 and Table 2). The difference might be determined by several factors.
   (a) It is well known, that a reduction of dislocation density and thereby a reduction of strain energy within the ferrite grains is the most important driving force for both processes, recovery and recrystallization [12]. In hot and cold rolled sheets, dislocation densities usually are larger at the surface than in the center of the sheets due to higher grain deformation introduced by additional shear.
   (b) Recrystallization is inhibited in case of strong α-fiber texture components $\{0\,0\,1\}\langle 1\,\bar{1}\,0\rangle$ and $\{1\,1\,2\}\langle 1\,\bar{1}\,0\rangle$ [20,21]. These texture components were particularly observed in the center of cold rolled sheets (Fig. 4), and therefore, yielded a slower recrystallization there (Fig. 1).
   (c) The spatial distribution of the constituents could also be of some importance. The ferritic–pearlitic band structure in the center of the sheets might yield growth conditions like in thin films [12]. The period of the band structure was found to be about 6–10 μm, which is only slightly larger than the distance between recrystallization nuclei. Hence, growth of newly formed recrystallized grains might be restricted to two dimensions. Also, the driving force for grain growth is diminished since grains are curved in only one rather than in two dimension and since grain boundaries might suffer pinning at the interfaces between constituents [12]. Actually, in the center of the sheets annealed at 740 °C ferrite grains were found to be slightly smaller than at the surface and showed a more pronounced pancake-type morphology (Fig. 5 and Table 2).
   (d) Finally, the precipitates found in hot and cold rolled sheets might yield pinning effects [12]. However, these precipitates were homogeneously distributed in the entire sheets, and therefore, cannot account for differences in recrystallization times.

(iii) The annealing experiments in the annealing simulator under variation of heating rates (Table 1, samples 5) indicated that recrystallization slightly dominated over recovery. A characteristic effect of strong recovery would be a reduction of the volume fraction of recrystallized ferrite at higher heating rates since time for recovery would be reduced. However, the opposite effect was found, i.e., the volume fraction of recrystallized ferrite increased at low heating rates since recrystallization already started during heating (Table 2).

4.3. Competition between recrystallization and phase transformation

Phase transformation was found to occur at intercritical temperatures larger than 710 °C, a pure austenitic annealing was found at temperatures larger than 860 °C. Similar as for recrystallization, a number of characteristic features shall be discussed on a more microscopic level. Coupling between recrystallization and phase transformation is of special interest.

(i) The incubation time for phase transformation decreased with increasing annealing temperature (Fig. 1). At austenitic temperatures, new equiaxed ferrite grains were formed with low orientation gradients and different texture. This is in agreement with phase transformation being a thermally activated

process and can be described in terms of nucleation and growth.

(ii) At low intercritical annealing temperatures of 740 °C, ferrite and martensite showed the same spatial distribution as ferrite and pearlite in the cold rolled sheets. Obviously, pearlite is affected by phase transformation before ferrite. However, at high intercritical annealing temperatures of 830 °C the ferrite–martensite band structure in the center of the sheets showed a stronger percolation. Finally, at austenitic annealing temperatures ferrite and martensite were found to be heterogeneously distributed in the entire sample.

(iii) The martensite volume fraction increased with annealing time unless phase transformation was completed (Figs. 1 and 3).

(iv) The martensite volume fraction increased with increasing cooling rate.

(v) The volume fraction of martensite was found to be larger for sheets annealed in the annealing simulator at 740 °C for 100–200 s than for sheets annealed in salt bath (Table 2, samples 3 and 4). Particularly, this observation seems to be in contradiction to the observation (iv) that the martensite volume fraction should be larger for high cooling rates as for annealing in salt bath. Also, annealing in salt bath at 740 °C for 30 s yielded a pure ferritic–pearlitic microstructure whereas annealing in the annealing simulator yielded a pure ferritic–martensitic microstructure (Table 2, samples 2 and 5). This observation can be attributed to two effects which are affected by a lower heating rate applied for annealing in the annealing simulator. First, it is known that for continuous annealing at low heating rates the phase transition temperature A_{c1} is closer to its minimum valid for thermodynamic equilibrium. Also, for a low heating rate there is more time for spherodization of pearlite which might be favorable for diffusion processes associated with phase transformation.

(vi) At the surface of the sheets, hardness after recrystallization at ferritic temperatures and the hardness minimum for annealing at low intercritical temperatures up to 740 °C were found to be equal. With increasing intercritical annealing temperatures the hardness minimum occurred after shorter annealing times and increased in magnitude. In summary, there is an overlap of recrystallization and phase transformation only at intercritical annealing temperatures above 740 °C.

(vii) In sheets intercritically annealed at 740 °C, the volume fraction of martensite and recrystallized ferrite showed and inverse correlation. The volume fraction of martensite (recrystallized ferrite) was larger (smaller) in the center than at the surface of the sheets. The results indicate a faster phase transformation of ferrite in the partially recrystallized sheet center layers than at the fully recrystallized surface. It is well known, that phase transformation in deformed ferrite should be faster than for recrystallized ferrite for several reasons [11,22]. First, the ferrite–austenite transformation is controlled by carbon and manganese diffusion [1], which is stronger in deformed materials due to a large number of dislocations and grain boundaries [22]. Second, deformed ferrite provides an increased number of nucleation sites and thus accelerates austenite formation [11]. Finally, deformation increases strain energy and thereby reduces the nucleation energy barrier introduced by the formation of austenite–ferrite interfaces [14,22]. Therefore, a reduction of strain energy introduced by deformation is a driving force for both processes, recrystallization and phase transformation. Particularly, after recrystallization the driving force for phase transformation is diminished.

In summary, for annealing in salt bath both processes, recrystallization and phase transformation, did not overlap at low intercritical annealing temperatures (Fig. 1). This offers a unique chance to study both processes separately in a systematic way. However, for annealing procedures with finite heating rates as applied for annealing in the annealing simulator or industrially hot-dip galvanizing both processes overlap even at low intercritical annealing temperatures and short annealing times, and therefore, a control of the competition between the processes will be more difficult. The results also revealed an interdependence of recrystallization and phase transformation, which can be attributed to a reduction of strain energy being a common driving force for both processes [14,22]. Recently, the importance of strain as driving force for ferrite–austenite phase transformations was shown with respect to the deformation induced ferrite transformation (DIFT) effect [23] in low carbon steels, where deformation of austenite is supposed to promote austenite to ferrite transformation. Similarly, it was shown that deformation applied during intercritical annealing promotes ferrite to austenite transformation [23]. In this work it is concluded that cold rolling applied before intercritical annealing also might promote ferrite to austenite transformation whereas recrystallization yields a diminishing effect. At high annealing temperatures, a reduction of strain will be insignificant as driving force for microstructure evolution compared to a reduction of free enthalpy during phase change. In future work, the interdependence between recrystallization and phase transformation due to strain and the role of ferrite–pearlite band structure in the center of cold sheets on recrystallization will be two main topics of research.

The experimental results presented here were complemented with numerical simulations to model the microstructure evolution during thermal treatment and the competition between recrystallization and phase transformation. Particularly, the basic Johnson–Mehl–Avrami–Kolmogorov (JMAK) equations were solved and a cellular automaton [24] was used for a sophisticated three-dimensional simulation. In a first step, recrystallization was numerically simulated for ferritic and low intercritical annealing temperatures. In a second step, the model of nucleation and grain growth, which form the basis of the JMAK model and the cellular automaton, was also applied to describe phase transformation at intercritical annealing temperatures. For this, the JMAK equations were extended to a system of differential equations which couple the evolution of the volume fractions of the various constituents with each other. Similarly, the cellular automaton was extended by additional input parameters such as nucleation density and grain boundary mobility of austenite. The numerical solutions of the JMAK equations and the computations by cellular automata yielded good agreement with respect to recrystallization and their extended versions yielded promising results with respect to phase transformation and will be presented elsewhere.

Acknowledgements

The authors thank Dr. M. Masimov and Dr. B. Springub (Salzgitter Mannesmann Forschung GmbH, Eisenhüttenstrasse 99, 38239 Salzgitter, Germany) for scientific and technical support. Financial support by the German Ministry for Education and Research under the project “Bauteilbewertung auf der Basis integraler Werkstoffmodellierung entlang der Prozesskette” (grant no. 03X0501E) is gratefully acknowledged.

References

[1] G.R. Speich, V.A. Demarest, R.L. Miller, Metallurgical Transactions A 12A (1981) 1419.
[2] W. Bleck, A. Frehn, J. Ohlert, Niobium Science and Technology: Proceedings of the International Symposium Niobium 2001, Niobium 2001 Limited, Orlando, FL, USA, 2001, pp. 727–752 (ISBN 9780971206809, 2002).

[3] R.K. Ray, Scripta Metallurgica 18 (1984) 1211.
[4] R.K. Ray, Materials Science and Engineering 77 (1986) 169.
[5] D.K. Mondal, R.K. Ray, Materials Science and Engineering A 158 (1992) 147.
[6] S.G. Chowdhury, E.V. Pereloma, D.B. Santos, Materials Science and Engineering A 480 (2008) 540.
[7] B. Gardey, S. Bouvier, V. Richard, B. Bacroix, Materials Science and Engineering A 400–401 (2005) 136.
[8] R.O. Rocha, T.M.F. Melo, E.V. Pereloma, D.B. Santos, Materials Science and Engineering A 391 (2005) 296.
[9] Y.S. Zheng, Z.G. Wang, S.H. Ai, Materials Science and Engineering A 176 (1994) 393.
[10] J. Qu, W. Dabboussi, F. Hassani, J. Nemes, S. Yue, Materials Science and Engineering A 479 (2008) 93.
[11] D.A. Porter, K.E. Easterling, Steel. A Handbook for Materials Research and Engineering Volume 1: Fundamentals, Springer, Berlin, Germany, 1992 (Chapters A3.5 and A7.4, ISBN 3-540r-r52968-3).
[12] F.J. Humphreys, M. Hatherly, Recrystallization and Related Annealing Phenomena, Elsevier, Oxford, GB, 2004.
[13] S.J. Kim, Y.G. Cho, C.S. Oh, D.E. Kim, M.B. Moon, H.N. Han, Materials and Design 30 (2009) 1251.
[14] M.A.F. Oliveira, A.M. Jorge Jr., O. Balancin, Scripta Materialia 50 (2004) 1157.
[15] D. Raabe, Steel Research 74 (2003) 327.
[16] S. Zaefferer, P. Romano, F. Friedel, Journal of Microscopy 230 (2008) 499.
[17] E. Demir, D. Raabe, N. Zaaferani, S. Zaefferer, Acta Materialia 57 (2009) 559.
[18] D. Raabe, K. Lücke, Material Science and Technology 9 (1993) 302.
[19] M. Hölscher, D. Raabe, K. Lücke, Acta Metallurgica 42 (1994) 879.
[20] D. Raabe, Physica Status Solidi (b) 181 (1994) 291.
[21] D. Raabe, Z. Zhao, S.J. Park, F. Roters, Acta Materialia 50 (2002) 421.
[22] D.A. Porter, K.E. Easterling, Phase Transformations in Metals and Alloys, Van Nostrand Reinhold, UK, Wokingham, GB, 1981 (Chapters 2.7, 5.2, and 5.8.3, ISBN 0-442r-r30439-0).
[23] H. Dong, X. Sun., Current Opinion in Solid State and Materials Science 9 (2005) 269.
[24] F. Roters, S. Schulz, N. Peranio, S. Lossau, O. Benevolenski, A. Butz, T. Rist, W. Schmitt, B. Springub, in: P. Hora (Ed.), Proceedings of the 7th International Conference and Workshop on Numerical Simulation of 3D Sheet Metal Forming Processes (NUMISHEET), Interlaken, CH, 2008, pp. 357–362 (ETH Zürich, CH, 2008).